Accepted Manuscript

Polarization-resolved terahertz imaging of intra- and inter-laminar damages in hybrid fiber-reinforced composite laminate subject to low-velocity impact

Junliang Dong, Alexandre Locquet, Nico F. Declercq, D.S. Citrin

PII: S1359-8368(16)00123-2

DOI: 10.1016/j.compositesb.2016.02.016

Reference: JCOMB 4054

To appear in: *Composites Part B*

Received Date: 29 June 2015

Revised Date: 22 January 2016

Accepted Date: 10 February 2016

Please cite this article as: Dong J, Locquet A, Declercq NF, Citrin DS, Polarization-resolved terahertz imaging of intra- and inter-laminar damages in hybrid fiber-reinforced composite laminate subject to low-velocity impact, *Composites Part B* (2016), doi: 10.1016/j.compositesb.2016.02.016.

Polarization-resolved terahertz imaging of intra- and inter-laminar damages in hybrid fiber-reinforced composite laminate subject to low-velocity impact

Junliang Dong[a,b,*], Alexandre Locquet[a,b], Nico F. Declercq[a,c], D. S. Citrin[a,b,**]

[a] *Georgia Tech-CNRS UMI2958, Georgia Tech Lorraine, 2 Rue Marconi, 57070 Metz, France*
[b] *School of Electrical and Computer Engineering, Georgia Institute of Technology, Atlanta, GA 30332, USA*
[c] *Woodruff School of Mechanical Engineering, Georgia Institute of Technology, Atlanta, GA 30332, USA*

Abstract

Terahertz imaging is applied to characterize a hybrid fiber-reinforced composite laminate subject to low-velocity impact in this study. The hybrid fiber-reinforced composite laminate comprises unidirectional glass/epoxy and carbon/epoxy plies with a cross-ply stack pattern. Both impact-induced intra- and inter-laminar damages are successfully detected, and the damage evolution throughout the thickness is also evaluated. The interaction between the terahertz polarization and carbon-fiber orientation is investigated in detail. Inter-laminar damage at the interface and the intra-laminar damage close to the same interface can be differentiated via polarization-resolved imaging. With a parameter fitting method based on multiple regression analysis, delamination is characterized quantitatively. Terahertz C- and B-scan images

*junliang.dong@gatech.edu
**david.citrin@ece.gatech.edu

clearly exhibit the propagation of the damage from the top to the bottom surface in three dimensions.

Keywords: D. Non-destructive testing, A. Hybrid, A. Polymer-matrix composites (PMCs), B. Impact behavior, Terahertz imaging

1. Introduction

Fiber-reinforced composites, such as carbon and glass fiber-reinforced composites, are increasingly being utilized in the industrial world to provide an alternative to conventional structural materials due to their high specific stiffness and strength, low weight and corrosion resistance. Hybrid fiber-reinforced composites, which combine two or more types of fibers in the same composites in order to benefit from the merits of each constituent fiber type, have also been used in many applications which need to meet both the requirements of cost and performance. Usually, one type of fiber in hybrid composites is high-modulus and/or high-cost, such as carbon or boron and the other type is low-modulus and/or low-cost, such as glass or Kevlar. The high-modulus fiber provides the stiffness and load bearing capability, whereas the low-modulus fiber makes the composite more damage tolerant and reduces the cost [1]. Therefore, hybrid composites can provide the balance of strength and stiffness, reduce the weight and/or cost while also improving fatigue resistance, fracture toughness, and impact resistance.

Fiber-reinforced composite laminates are vulnerable to impact. The resulting impact-induced damage in laminates involves a combination of intra-laminar damage (such as matrix cracking or fiber/matrix debonding and fiber distortion/fracture) and inter-laminar damage, which leads to the sep-

aration of adjacent plies (delamination) [2]. High-velocity impact, with speed up to 2500 m/s, results in perforations and the breakage of fibers. On the other hand, low-velocity impact damage, with energy in range of 5 to 25 J or with speed between 5 m/s and 15 m/s, sometimes invisible on the surface, involves a combination of matrix cracking and delamination within the laminate [3]. Delaminations are considered the most important failure mechanism, because they can severely degrade the strength and the integrity of the structure, and may propagate undetected during service, leading to a significant decrease in stability and durability. For these reasons, there is an urgent need for advanced nondestructive evaluation (NDE) techniques for impact damage in fiber-reinforced composite laminates over component lifecycle—during service and maintenance.

Various NDE techniques have been developed for impact damage detection in composite structures over the last few decades, such as shearography [4], ultrasonic testing [5, 6], eddy current [7], thermography [8] and X-ray computed tomography [9]. However, not all these methods can provide information in depth to observe the morphology and evolution of the impact damage throughout the entire thickness of the laminate [3]. Ultrasonic C-scans in pulse-echo mode can be utilized for imaging the evolution of impact damage in carbon fiber-reinforced composite laminate [10]; however, the attenuation of ultrasonic waves in glass fiber-reinforced composite laminate is prohibitively high so that the operating frequency cannot in practice typically exceed 5 MHz, limiting the spatial resolution [11]. Ultrasonic C-scans also frequently suffer from the problem of liquid coupling. The spatial resolution of X-ray computed tomography is high and can provide three-dimensional

imaging; however, it is difficult to implement for large composite laminates and, as X-rays are ionizing radiation, it carries significant health risks.

Terahertz (THz) imaging, as a new promising NDE technique, can provide a noninvasive, noncontact, and nonionizing method to characterize nonmetallic materials. The THz portion of the electromagnetic spectrum extends from approximately 100 GHz to 10 THz, and lies between the microwaves and infrared; the wavelength range in this region is 3 mm down to 3 μm. THz waves can penetrate numerous nonmetallic materials which may be opaque in the range of visible and infrared light [12]. Moreover, as nonionizing radiation, THz waves present minimal known health risks [13]. Due to these remarkable properties, THz waves have already been used to characterize various types of defects, such as impact damage, voids, delamination, and intrusions in glass fiber-reinforced composites [11, 14, 15, 16, 17]. Moreover, THz waves can also be applied to measure the optical material parameters [18] and the fiber orientation [19] for glass fiber-reinforced composites. However, the conductivity of carbon fibers hinders the applications of THz waves to carbon fiber-reinforced composites to some extent, and THz waves have to date only been demonstrated to detect the impact-induced matrix cracking on the surface [20].

In this study, THz imaging is firstly applied to a hybrid fiber-reinforced composite laminate, comprised of unidirectional glass/epoxy and carbon/epoxy laminae with a cross-ply stack pattern. The evolution of intra-laminar and inter-laminar damage throughout the thickness of the laminate (1.65 mm) subject to low-velocity impact is evaluated. Inter-laminar damage at the interface and the intra-laminar damage close to the same interface can be

differentiated by taking advantage of the sensitivity of the carbon-fiber orientation to the THz polarization. THz C- and B-scan images are obtained to exhibit the propagation of the damage from the top to the bottom surface in three dimensions.

2. Theoretical Background

The conductivity of carbon fibers severely limits the penetration ability of THz waves into the material. For unidirectional carbon fiber-reinforced composites, the conductivity is anisotropic and depends on the THz polarization and fiber orientation, which can be expressed as [21]

$$\sigma(\theta) = \sigma_l \cos^2\theta + \sigma_t \sin^2\theta \tag{1}$$

where θ is the angle between the THz polarization and fiber orientation and σ_l and σ_t are the longitudinal and transverse conductivities, respectively. Along the fiber direction, the electric current flows through the carbon fibers, so the longitudinal conductivity depends on the conductivity of carbon fibers σ_f and on the fiber volume fraction ν_f,

$$\sigma_l \approx \sigma_f \nu_f \tag{2}$$

For the transverse conductivity, because the resin material is nonconductive, the flow of electric current only occurs due to random contact between adjacent carbon fibers, which depends on the manufacturing process and the quality of the composites [21]. Therefore, the longitudinal conductivity is much higher than the transverse conductivity. Based on the literature [22],

longitudinal conductivity rangs from 1×10^4 S/m to 6×10^4 S/m, and the transverse conductivity varies from 2 S/m to 600 S/m.

By analyzing the electric conductivity, one finds that (1) when the THz polarization is parallel to the orientation of carbon fibers, the electric conductivity is maximum and the THz reflectivity also reaches the maximum; (2) when the THz polarization is perpendicular to the carbon fibers, conductivity and reflectivity achieve their minimum. The ideal amplitude reflection coefficient $R_{\_ideal}$ can be expressed as

$$R_{\_ideal} \approx 1 - \sqrt{\frac{2\omega\epsilon_0}{\sigma}} \tag{3}$$

where ω is the THz frequency, and ϵ_0 is the permittivity of free space. The reflection coefficient approximately equals to 1 when THz polarization is parallel to the carbon-fiber orientation.

Monitoring the reflection coefficient across the surface of carbon fiber composites with THz imaging can be utilized as a method to characterize the impact damage on the surface. When carbon fiber-reinforced composites suffer from impact damage, carbon fiber distortion and fracture will occur in the damage area, which will lead to spatial variation of the reflection coefficient as well as the polarization anisotropy. The reflection coefficient in regions with and without impact damage can be more easily distinguished with polarization parallel to the carbon-fiber orientation [23].

3. Sample

The tested sample is a cross-ply hybrid fiber-reinforced composite laminate, shown in Fig. 1. The dimension of the laminate is 120 mm (length:

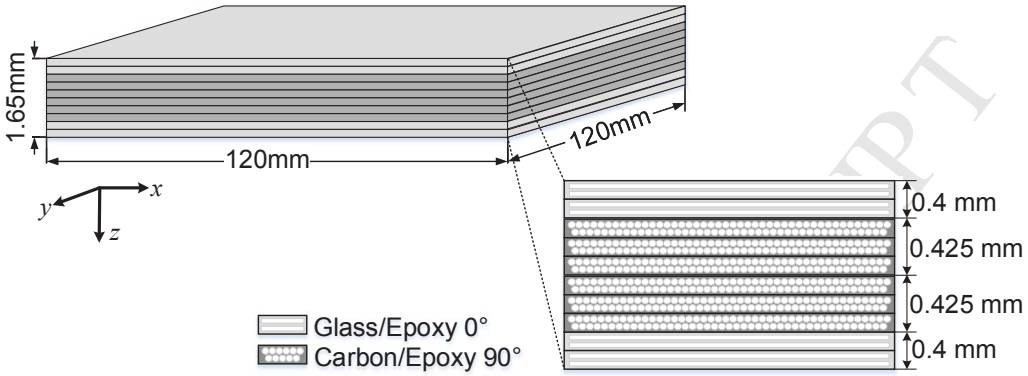

Figure 1: Schematic diagram of hybrid fiber-reinforced composite sample indicating dimensions and internal structure.

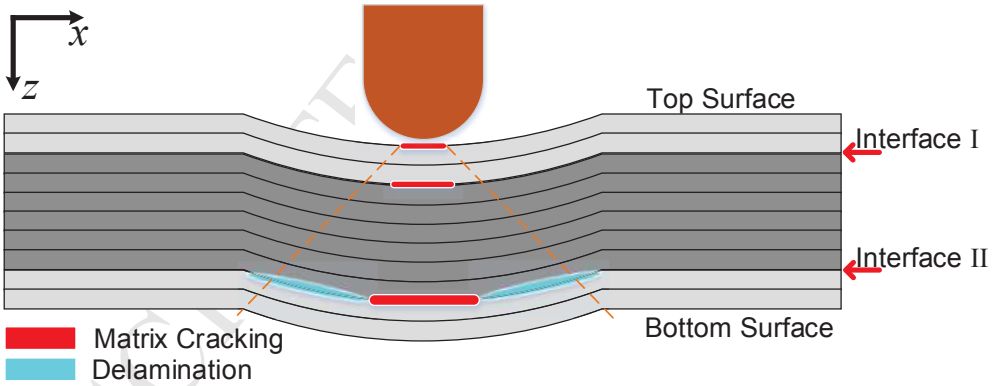

Figure 2: Schematic diagram (edge view) of sample subjected to low-velocity impact damage with highlighted damage types.

x direction) × 120 mm (width: y direction) × 1.65 mm (thickness: z direction). The laminate is formed from prepregs of unidirectional E-glass fibers with epoxy resin, and prepregs of unidirectional carbon fibers with epoxy resin. For the prepreg of glass/epoxy, the fiber volume fraction is 60 vol.% and the resin content is 33 wt.%, the orientation of the glass fibers is along the direction of length (x direction); for the prepreg of carbon/epoxy, the fiber volume fraction is 60 vol.% and the resin content is about 42 wt.%, the orientation of the carbon fibers is along the direction of width (y direction). The stacking sequence of the laminate is $[0\,^{\circ G}_{2}/90\,^{\circ C}_{3}]_s$, corresponding to the thicknesses $[0.400\text{ mm}/0.425\text{ mm}]_s$. The electric conductivity of the carbon fiber is 5.88×10^4 S/m in our case. Damage was generated by controlled free-fall impact: an impactor of 50 g struck the center of the top surface of the laminate at a speed of 9.5 m/s, schematically shown in Fig. 2.

This damaged sample was firstly scanned with ultrasonic waves to get initial knowledge of the damage pattern and also to provide a point of comparison for the THz imaging results. A customer-designed ultrasonic scanner fabricated by Inspection Technology Europe BV was used for the ultrasonic C-scan experiment. The transducers chosen for this investigation are focused immersion transducers with a manufacturer-provided central frequency of 5 MHz, since this frequency provides a balance between the attenuation and resolution. Ultrasonic C-scans were performed on the sample with water coupling under both transmission (pitch-catch) mode and reflection (pulse-echo) mode over an area of 50 mm × 30 mm with a 0.2 mm scan step size. The ultrasonic C-scan in transmission, shown in Fig. 3(a), exhibits the accumulative damage pattern through the sample, since the surface bending,

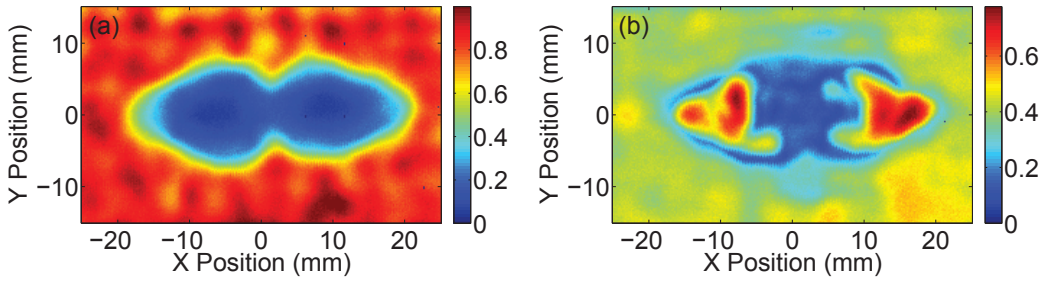

Figure 3: Ultrasonic C-scan results (a) in transmission and (b) in reflection modes. The ultrasonic waves are incident from the top surface of the sample. The contrast is based on the absolute value of the amplitude of the second-round signal in transmission and the second echo in reflection.

inter- and intra-laminar damages all lead to the attenuation of ultrasonic waves; the ultrasonic C-scan in reflection, shown in Fig. 3(b), can highlight the inter-laminar damage region, since the delamination (gap) leads to higher reflection.

However, due to the limited axial resolution, ultrasonic C-scans cannot provide information in depth to observe the morphology and evolution of the impact damage throughout the thickness of this laminate. Therefore, polarization-resolved THz imaging is performed in the following.

4. Experiment

The THz time-domain spectroscopy (TDS) system (Teraview TPS Spectra 3000), which is employed in this study, is shown schematically in Fig. 4. The GaAs photoconductive antenna is excited by an ultrafast (femtosecond) laser to produce roughly single-cycle THz pulses with bandwidth extending from 60 GHz to 3 THz. The ultrafast laser used here is an Er-doped fiber

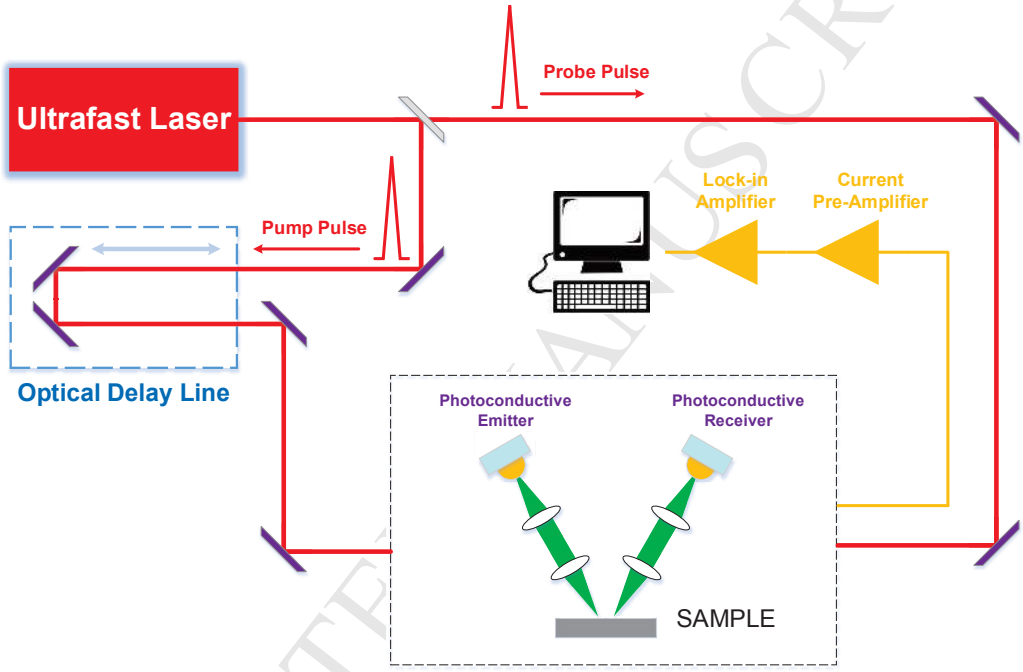

Figure 4: Schematic diagram of THz time-domain spectroscopy (TPS) system in reflection mode.

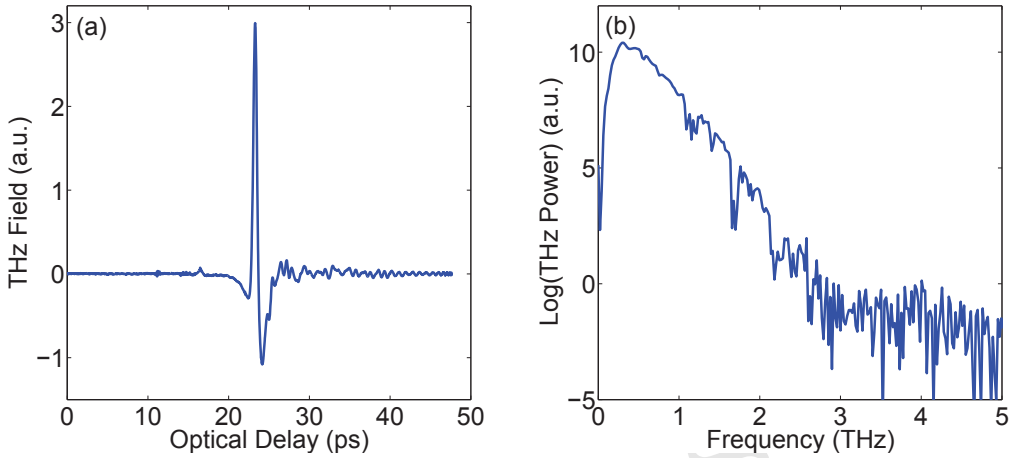

Figure 5: Time-domain waveform (a) and frequency spectrum (b) of the THz reference signal

laser that emits 780 nm pulses with sub-100 femtosecond pulse duration at a repetition rate of 100 MHz and has an average output power in excess of 65 mW. Coherent detection of the THz radiation is performed in a similar photoconductive antenna circuit. By gating the photoconductive gap with a femtosecond pulse synchronized to the terahertz emission, a current proportional to the THz electric field is measured. By varying the optical path length, the THz time domain can be sampled, resulting in both amplitude and phase information on a sub-picosecond timescale.

THz imaging is performed in reflection mode at almost normal incidence. Before imaging the sample, a THz reference signal was recorded by setting a metal plate at the sample position. The time domain waveform and the spectrum of this reference signal are shown in Fig. 5. The THz pulse [Fig. 5(a)] is composed of approximately one electromagnetic cycle, and its duration is a few picoseconds. The spectrum [(Fig. 5(b)], obtained by Fourier transforming

the temporal pulse, extends from ∼100 GHz to ∼3 THz. Pronounced atmospheric water-absorption lines can be observed [24]. The power of the THz radiation is below 1 μW so no thermal strain is induced in the sample.The sample is raster-scanned by a set of motorized stages moving in x and y directions with a 0.2 mm spatial step size over the center area (50 mm × 30 mm) of the sample plane. THz waves cannot penetrate the entire sample thickness due to the carbon fibers in the central layer. Therefore, we separately imaged the sample from both the top and bottom surfaces. In order to consider the interaction between the THz polarization and carbon-fiber orientation, the THz polarization was set first in the x direction (perpendicular to the carbon-fiber orientation). After completing the scans from both surfaces, the polarization was rotated to the y direction (parallel to the carbon-fiber orientation). In total, four sets of images were acquired in this study.

5. Results and Discussion

Based on the sample structure, we expect THz temporal waveforms reflected off the various interfaces in Fig. 6. In the case of a region without impact damage [Fig. 6(a)], the first echo is determined by the Fresnel reflection at the surface of the sample, and the second echo corresponds reflection at the interface between the glass/epoxy and carbon/epoxy layers with multiple reflections inside the sample following. For normal incidence on an interface between two media with refractive indices n_i and n_j , the amplitude reflection coefficients r_{ij} and transmission coefficients t_{ij} are

$$r_{ij} = \frac{n_i - n_j}{n_i + n_j} \tag{4}$$

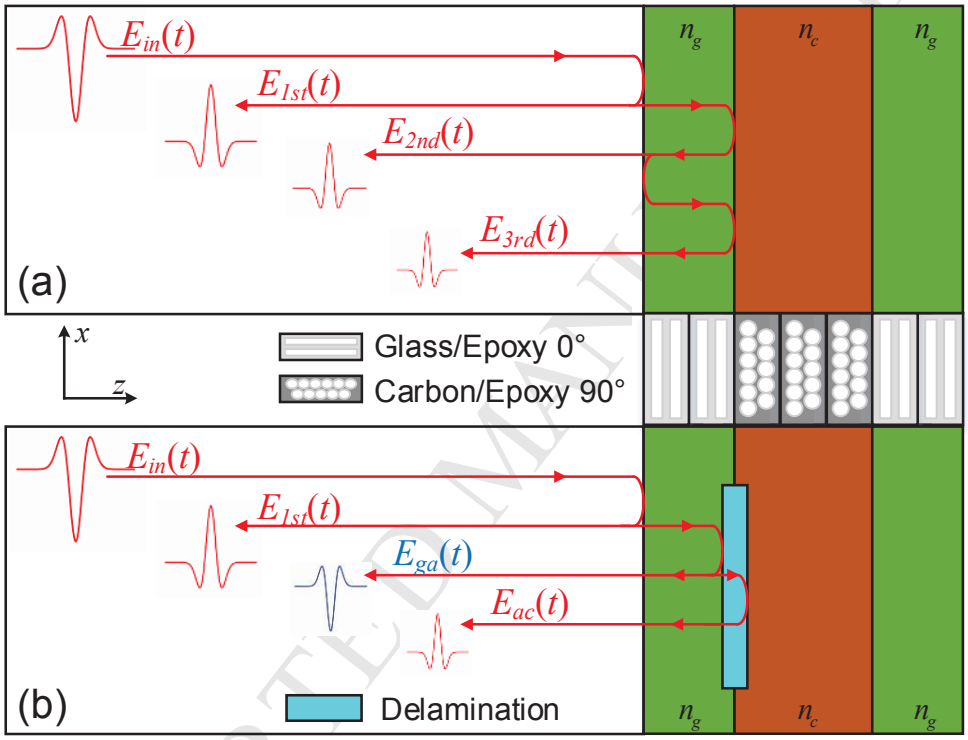

Figure 6: Estimated reflected THz waveforms (a) in undamaged region and (b) in region with delamination.

$$t_{ij} = \frac{2n_i}{n_i + n_j} \tag{5}$$

In our study, we consider the THz reference signal shown in Fig. 5(a) as the incident THz pulse $E_{THz}(t)$, and we also neglect the negligibe dispersion in the relevant spectral range. The reflected THz waveform is

$$E_{THz}(t) = E_{1st}(t) + E_{2nd}(t) + E_{3rd}(t) \tag{6}$$

with

$$E_{1st}(t) = r_{ag}E_{in}(t) \tag{7}$$

$$E_{2nd}(t) = t_{ag}r_{gc}t_{ga}E_{in}(t - \frac{2n_g d}{c})e^{-2\alpha d} \tag{8}$$

$$E_{3rd}(t) = t_{ag}r_{gc}r_{ga}r_{gc}t_{ga}E_{in}(t - \frac{4n_g d}{c})e^{-4\alpha d} \tag{9}$$

where c is the *in vacuo* speed of light, d is the thickness of the glass/epoxy layer, n_g is the refractive index of glass/epoxy layer, α is the absorption coefficient in the glass/epoxy layer, t_{ag} and t_{ga} are transmission coefficients from air to glass/epoxy and glass/epoxy to air, r_{gc} are r_{ga} reflection coefficients from glass/epoxy to carbon/epoxy and glass/epoxy to air, and we only consider one multiple reflection.

Typical THz waveforms with polarization parallel and perpendicular to the carbon-fiber orientation from the undamaged region in experiments are shown in Fig. 7. The significant difference of the amplitudes of the second echoes, which reflect from the interface between the glass/epoxy and carbon/epoxy plies, illustrates the change of reflection coefficient under different polarization. In addition to the difference in amplitude, a temporal delay of the second echoes for the two polarizations is also observed, indicating that the group velocity depends on polarization in the glass/epoxy plies.

The refractive index of glass/epoxy n_g can be estimated from the time delay ΔT between the first and second echoes and the thickness of the glass/epoxy layer d as

$$n_g = \frac{c\Delta T}{2d} \tag{10}$$

In our case, with the polarization parallel to the glass fibers, the refractive index is $n_{g,\parallel}$=2.124; with polarization perpendicular to the glass fibers, the refractive index is $n_{g,\perp}$=1.950. This polarization anisotropy underlies previously observed THz birefringence in unidirectional glass fiber-reinforced composites [25].

First, we discuss the THz images when the THz pulse is incident on the top surface of the sample. Polarization-resolved C-scans obtained from the top surface and interface I are shown in Fig. 8 and Fig. 9. The selected contrast mechanism for all the THz images in this study is the peak-to-valley amplitude difference of the corresponding echoes. Impact damage on the surface can be clearly seen in Fig. 8, and there is no significant difference between C-scans with different polarization. However, polarization dependence in the C-scans associated with interface I is pronounced due to influence of carbon fibers, as shown in Fig. 9. Impact-induced matrix cracking and fiber distortion/fracture in the carbon/epoxy layer lead to the decrease of the reflection coefficient at interface I for both perpendicular and parallel polarizations. By contrast, we observe parallel polarization is more sensitive to the region with fiber distortion/fracture, and leads to a further decrease of the reflected pulse amplitude compared with that for perpendicular polarization, which provides better contrast for locating the damage area in C-scan. B-scan images across the section y=0 provide depth information,

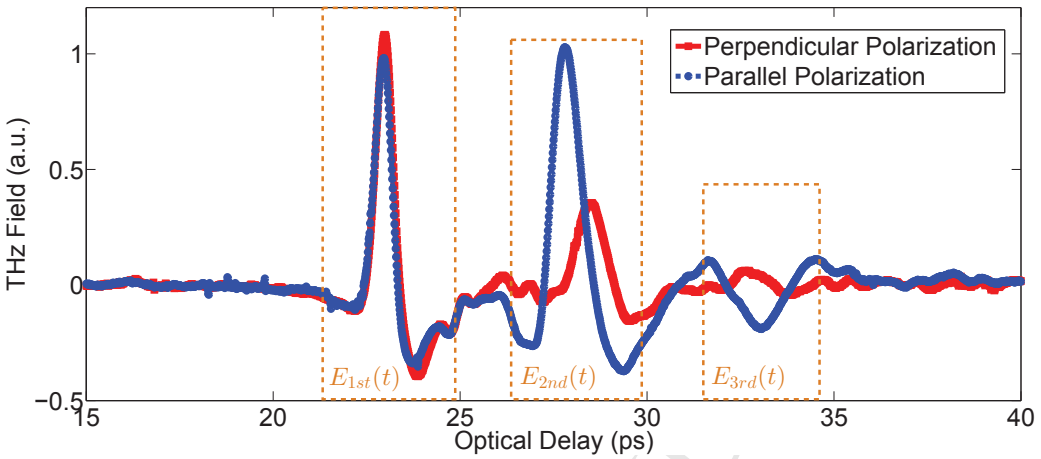

Figure 7: Typical time-of-flight waveforms from an undamaged region with THz polarization parallel and perpendicular to the carbon fibers.

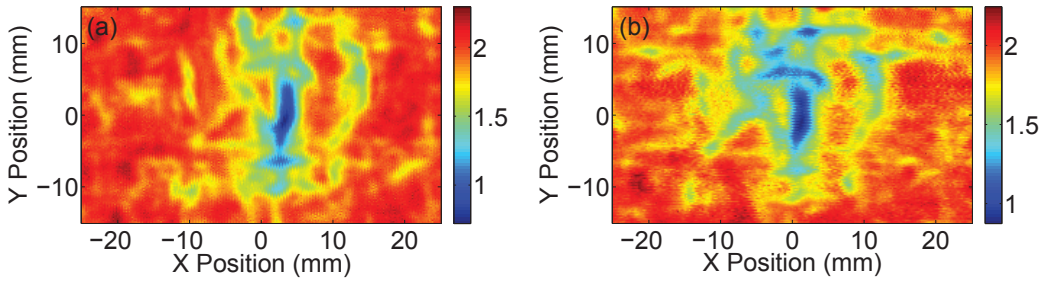

Figure 8: THz C-scans of the top surface with polarization perpendicular (a) and parallel (b) to the carbon-fiber orientation.

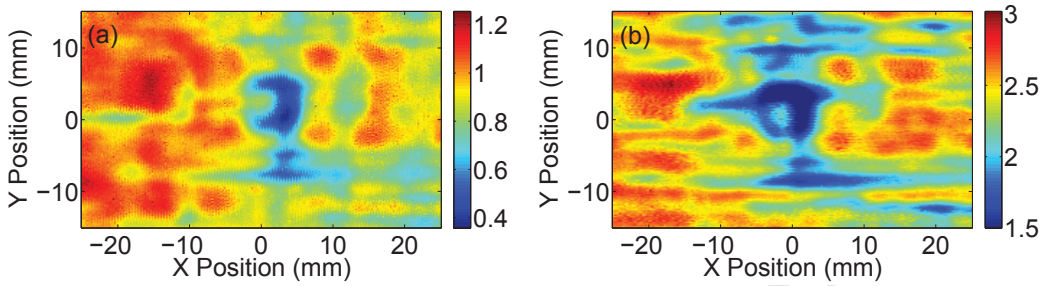

Figure 9: THz C-scans of the Interface I with polarization perpendicular (a) and parallel (b) to the carbon-fiber orientation.

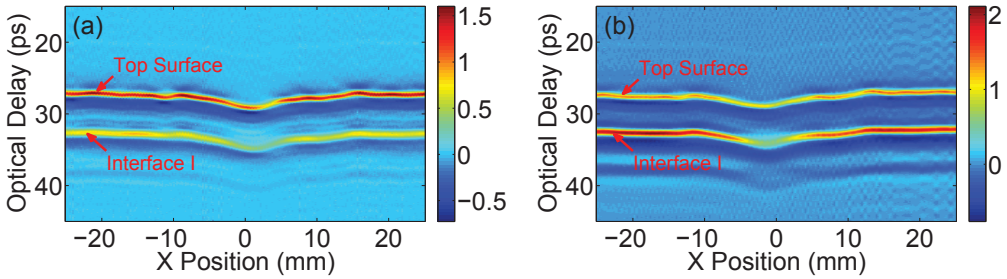

Figure 10: THz B-scans incident on the top surface (along section y=0) and with polarization perpendicular (a) and parallel (b) to the carbon-fiber orientation.

as shown in Fig. 10. Indentation on the surface and damaged regions can also be located in THz B-scans. The combination of the THz C-scan and B-scan images exhibit the evolution of the impact-induced damage from the top surface to the first interface between glass/epoxy and carbon/epoxy in three dimensions.

Images incident on the bottom surface of the sample are now discussed in the following. Fig. 11 shows C-scans of the bottom surface, which evidence the protrusion on the bottom surface introduced by the propagation of the impact damage from the top surface. Again, no significant polarization dependence is observed for this glass/epoxy layer. C-scans of interface II between the carbon/epoxy and glass/epoxy layers are shown in Fig. 12. Unlike the previous results, the C-scans in this case show quite different damage patterns for the two polarizations. For parallel polarization, the damaged region shows lower contrast due to the existence of matrix cracking and fiber distortion/fracture, which is consistent with the previous results. However, for perpendicular polarization, the damaged region shows higher contrast. This higher contrast indicates the existence of an air gap originating in the separation of the carbon/epoxy and glass/epoxy plies, i.e., delamination.

The THz waveforms in region of delamination can also be estimated, as shown in Fig. 6(b). Usually, the air gap associated with the delamination is thin; thus, the second echo $E_{2nd}(t)$ received is the superposition of the two echoes reflected from the glass/epoxy-air interface $E_{ga}(t)$ and from the

air-carbon/epoxy interface $E_{ac}(t)$, which can be expressed as

$$\begin{aligned} E_{2nd}(t) &= E_{ga}(t) + E_{ac}(t) \\ &= t_{ag} r_{ga} t_{ga} E_{in}(t - \frac{2n_g d'}{c}) e^{-2\alpha d'} \\ &+ t_{ag}^2 r_{ac} t_{ga}^2 E_{in}(t - \frac{2n_g d'}{c} - \frac{2d_{gap}}{c}) e^{-2\alpha d'} \end{aligned} \tag{11}$$

where d' is the thickness of the glass/epoxy layer with deformation due to the impact damage, d_{gap} is the thickness of the air gap, and the absorption in the narrow air gap is neglected. Because of the opposite sign of the reflection coefficient r_{ga} at the interface between glass/epoxy and air gap, the THz pulse will be inverted at this interface.

The change in the peak-to-valley difference of the second echo in the damaged region depends mainly on two factors: (1) the thickness of the air gap d_{gap} (a narrower air gap leads to a smaller difference in the peak-to-valley differences due to partial cancellation of the negative and positive peaks) and (2) the reflection coefficient r_{ga} (impact-induced matrix cracking and fiber distortion/fracture in the carbon/epoxy will lower the value of the reflection coefficient, which will further decrease the peak-to-valley difference). Therefore, for C-scans with perpendicular polarization, the thickness of the delamination dominates the change of the contrast, and the C-scans reveal the delamination area at the interface. For C-scans with parallel polarization, the reflection coefficient at the interface dominates the change of the contrast. Thus, the C-scan in this case evidences the matrix cracking and fiber distortion in the carbon/epoxy layer.

We implemented a numerical parameter fitting method based on multiple regression analysis [26] to estimate the delamination thickness and the

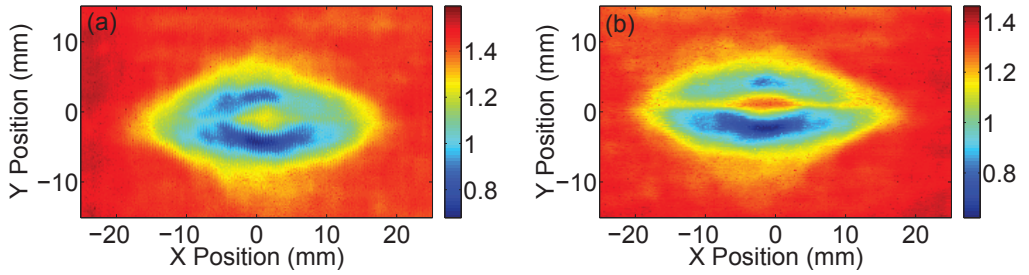

Figure 11: THz C-scans of the bottom surface with polarization perpendicular (a) and parallel (b) to the carbon fiber orientation.

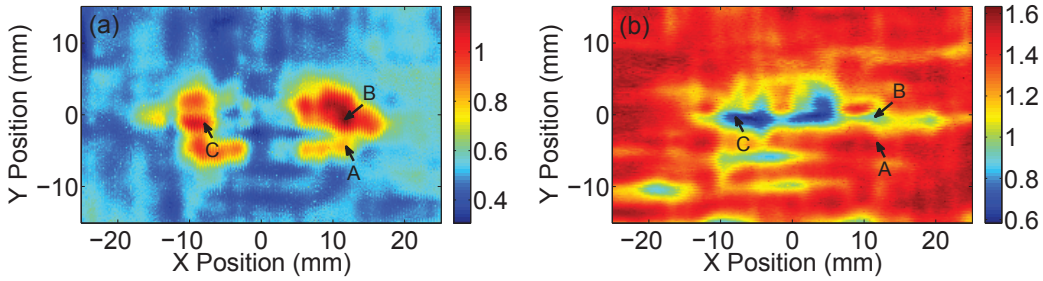

Figure 12: THz C-scans of the Interface II with polarization perpendicular (a) and parallel (b) to the carbon fiber orientation.

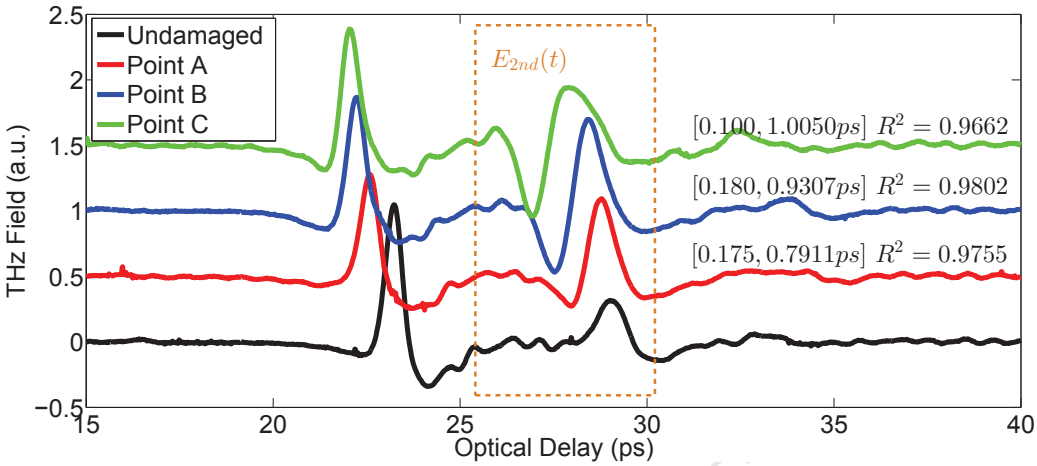

Figure 13: Temporal waveforms for perpendicular THz polarization at selected positions on sample (see Fig. 11).

reflection coefficient at the interface between the air gap and carbon/epoxy layer. The measured second echo is considered as the objective function, and a model function E_{model} is defined based on the equation (11) to stimulate the objective function as

$$E_{model} = a_1 E_{in}(t - t_1) + a_2 E_{in}(t - t_1 - \Delta t) \tag{12}$$

where a_1, a_2, t_1 and Δt are the regression parameters. Initial values should be carefully set so that the regression analysis can converge to a characteristic global minimum. Then multiple regression analysis with least-squares minimization is performed to estimate the regression parameters. In our case, our desired parameters are a_2 and Δt, which contain the information about the delamination thickness and the reflection coefficient between the air gap and the carbon/epoxy layer. Fig. 13 shows the temporal waveforms with perpendicular THz polarization at selected points (shown in Fig. 12) and the estimated parameters $[a_2, \Delta t]$ obtained by the multiple regression

analysis. The coefficient of determination R^2 is also used here to provide information about the goodness of fit of the regression model function [27]. The corresponding delamination thicknesses are 118.67 μm, 139.61 μm and 150.08 μm for Points A to C respectively. Although d_{gap} is largest at Point C, the signal here does not exhibit the highest contrast in Fig. 12(a). The reason is that a_2 is smaller at Point C compared with at Point B, indicating matrix cracking and fiber distortion is more severe at Point C, which is also observed in Fig. 12(b).

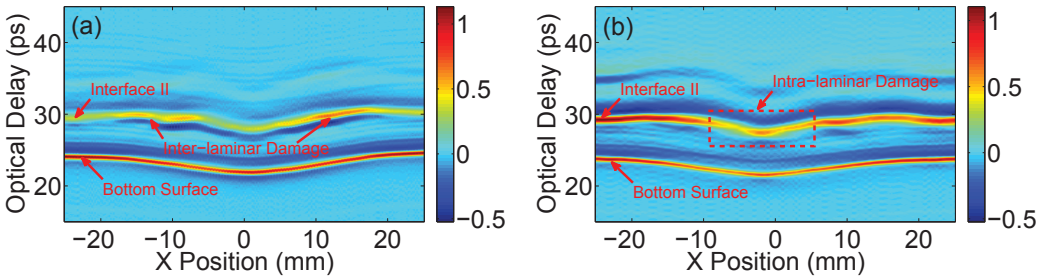

Figure 14: B-scans incident from the bottom surface (along section y=0) and with polarization perpendicular (a) and parallel (b) to the carbon-fiber orientation.

B-scans obtained incident from the bottom surface are shown in Fig. 14. Typical damage features can be observed in depth, including surface bending, inter- and intra-laminar damages. Therefore, the total set of C- and B-scans exhibits the evolution of the impact-induced damage from the top to the bottom surface in three dimensions, which fits quite well with theoretical simulation results in Ref. [28, 29]. The size of the delamination area can be calculated by applying the '50% rule' to the THz C-scan [11], and the thickness of the delamination can also be obtained with the parameter fitting method based on multiple regression analysis. Therefore, the delamination

can be characterized quantitatively in three dimensions.

6. Conclusion

In this study, polarization-resolved THz imaging was explored to characterize the evolution of the damage in a hybrid fiber-reinforced composite laminate subjected to low-velocity impact. The hybrid fiber-reinforced composite laminate is composed of unidirectional glass/epoxy and carbon/epoxy laminae with cross-ply stack pattern. Both intra-laminar (matrix cracking and fiber distortion/fracture) and inter-laminar damages (delamination) in the sample are successfully detected. THz C-scans exhibit the great capability of evaluating the morphology of the damage at various interfaces, which provide a clear representation of the propagation of the damage throughout the thickness. Moreover, depth information is obtained from THz B-scans, together with a parameter fitting method based on multiple regression analysis, enabling us to characterize the delamination quantitatively.

We also studied the effect of THz polarization in distinguishing features around the interface, where both intra- and inter-laminar damages exist. Inter-laminar damage at the interface and the intra-laminar damage close to the same interface, which most NDE techniques are ill-suited to resolve, are successfully differentiated by exploiting the sensitivity of the carbon-fiber orientation to the THz polarization.

Acknowledgment

We gratefully acknowledge the financial support of the Conseil Régional de Lorraine, and the Fonds Européen de Développement Régional (FEDER).

References

[1] Sevkat E, Liaw B, Delale F. Drop-weight impact response of hybrid composites impacted by impactor of various geometries. Materials & Design. 2013;52(0):67-77.

[2] Feng D, Aymerich F. Finite element modelling of damage induced by low-velocity impact on composite laminates. Composite Structures. 2014;108(0):161-71.

[3] Gaudenzi P, Bernabei M, Dati E, De Angelis G, Marrone M, Lampani L. On the evaluation of impact damage on composite materials by comparing different NDI techniques. Composite Structures. 2014;118(0):257-66.

[4] Kadlec M, Rek R. A Comparison of Laser Shearography and C-Scan for Assessing a Glass/Epoxy Laminate Impact Damage. Appl Compos Mater. 2012;19(3-4):393-407.

[5] Margueres P, Meraghni F, Benzeggagh ML. Comparison of stiffness measurements and damage investigation techniques for a fatigued and post-impact fatigued GFRP composite obtained by RTM process. Composites Part A: Applied Science and Manufacturing. 2000;31(2):151-63.

[6] Margueres P, Meraghni F. Damage induced anisotropy and stiffness reduction evaluation in composite materials using ultrasonic wave transmission. Composites Part A: Applied Science and Manufacturing. 2013;45:134-44.

[7] He Y, Tian G, Pan M, Chen D. Non-destructive testing of low-energy impact in CFRP laminates and interior defects in honeycomb sandwich

using scanning pulsed eddy current. Composites Part B: Engineering. 2014;59(0):196-203.

[8] Usamentiaga R, Venegas P, Guerediaga J, Vega L, López I. Feature extraction and analysis for automatic characterization of impact damage in carbon fiber composites using active thermography. NDT & E International. 2013;54(0):123-32.

[9] Tan KT, Watanabe N, Iwahori Y. X-ray radiography and micro-computed tomography examination of damage characteristics in stitched composites subjected to impact loading. Composites Part B: Engineering. 2011;42(4):874-84.

[10] Saito H, Kimpara I. Evaluation of impact damage mechanism of multi-axial stitched CFRP laminate. Composites Part A: Applied Science and Manufacturing. 2006;37(12):2226-35.

[11] Dong J, Kim B, Locquet A, McKeon P, Declercq N, Citrin DS. Nondestructive evaluation of forced delamination in glass fiber-reinforced composites by terahertz and ultrasonic waves. Composites Part B: Engineering. 2015;79(0):667-75.

[12] Mittleman D. Sensing with terahertz radiation / Daniel Mittleman, (ed.): Berlin ; New York : Springer, c2003, 2003.

[13] Wilmink G, Grundt J. Current State of Research on Biological Effects of Terahertz Radiation. J Infrared Milli Terahz Waves. 2011;32(10):1074-122.

[14] Rutz F, Koch M, Khare S, Moneke M, Richter H, Ewert U. Terahertz quality control of polymeric products. Int J Infrared Milli Waves. 2006;27(4):547-56.

[15] Ospald F, Zouaghi W, Beigang R, Matheis C, Jonuscheit J, Recur B, et al. Aeronautics composite material inspection with a terahertz time-domain spectroscopy system. Optical Engineering. 2013;53(3):031208.

[16] Stoik C, Bohn M, Blackshire J. Nondestructive evaluation of aircraft composites using reflective terahertz time domain spectroscopy. NDT & E International. 2010;43(2):106-15.

[17] Palka N, Miedzinska D. Detailed non-destructive evaluation of UHMWPE composites in the terahertz range. Opt Quant Electron. 2014;46(4):515-25.

[18] Naito K, Kagawa Y, Utsuno S, Naganuma T, Kurihara K. Dielectric properties of woven fabric glass fiber reinforced polymer-matrix composites in the THz frequency range. Composites Science and Technology. 2009;69(1112):2027-9.

[19] Jördens C, Scheller M, Wietzke S, Romeike D, Jansen C, Zentgraf T, et al. Terahertz spectroscopy to study the orientation of glass fibres in reinforced plastics. Composites Science and Technology. 2010;70(3):472-7.

[20] Bezborodov VI, Kiseliov VK, Kosiak OS, Kuleshov YM, Nesterov P-K, Yanovsky MS. Quasi-optical sub-terahertz internal reflection reflec-

tometer for non-destructive testing of carbon fiber reinforced plastics. Telecommunications and Radio Engineering. 2014;73(1):83-93.

[21] Athanasopoulos N, Kostopoulos V. Prediction and experimental validation of the electrical conductivity of dry carbon fiber unidirectional layers. Composites Part B: Engineering. 2011;42(6):1578-87.

[22] Kwang-Hee I, Hsu DK, Chien-Ping C, Barnard DJ, Jong-An J, In-Young Y. Terahertz Wave Approach and Application on FRP Composites. Advances in Materials Science & Engineering. 2013:1-10.

[23] Yang S-H, Kim K-B, Oh HG, Kang J-S. Non-contact detection of impact damage in CFRP composites using millimeter-wave reflection and considering carbon fiber direction. NDT & E International. 2013;57(0):45-51.

[24] Dong J, Locquet A, Citrin DS. Enhanced Terahertz Imaging of Small Forced Delamination in Woven Glass Fibre-reinforced Composites with Wavelet De-noising. J Infrared Milli Terahz Waves. 2015:1-13.

[25] Palka N, Krimi S, Ospald F, Miedzinska D, Gieleta R, Malek M, et al. Precise Determination of Thicknesses of Multilayer Polyethylene Composite Materials by Terahertz Time-Domain Spectroscopy. J Infrared Milli Terahz Waves. 2015;36(6):578-96.

[26] Yasuda T, Iwata T, Araki T, Yasui T. Improvement of minimum paint film thickness for THz paint meters by multiple-regression analysis. Applied Optics. 2007;46(30):7518-26.

[27] Hines WW. Probability and statistics in engineering / William W. Hines ... [et al.]: Hoboken, NJ : Wiley, c2003. 4th ed., 2003.

[28] Tan W, Falzon BG, Chiu LNS, Price M. Predicting low velocity impact damage and Compression-After-Impact (CAI) behaviour of composite laminates. Composites Part A: Applied Science and Manufacturing. 2015;71(0):212-26.

[29] Zhang J, Zhang X. Simulating low-velocity impact induced delamination in composites by a quasi-static load model with surface-based cohesive contact. Composite Structures. 2015;125(0):51-7.